Characterization of the intima layer of the aorta by Digital Image Correlation in dynamic traction up to failure

Sophie Litlzer[1], Philippe Vezin[1]

Abstract The mechanical properties of the aortic wall are important to develop a biofidelic finite element model. In this study, the influence of the location on the deformation characteristics along the descending aorta was investigated on 53 samples of pig aortic specimens. Uniaxial tensile tests up to failure were carried out at a strain rate of 68 s^{-1} in the longitudinal direction. Cauchy stress-true strain relationships were determined and compared for 4 different locations from the aortic arch to the abdominal aorta. Digital Image Correlation (DIC) was used to determine the Green-Lagrange full field strain. The experiments showed that the Cauchy stress vs. true strain relationship is more representative of the large deformation of the tissue than the engineering stress-strain curves. The influence of the location was not found to be significant for engineering stress (mean value 1.2±0.3 MPa) whereas a significant difference ($p<0.005$) between the aortic arch (3.4 MPa) and the thoracic aorta (2.7 MPa) was found for the Cauchy stress. The Green Lagrange strain at rupture measured for the aortic arch was found to be significantly higher (4.0) compared to the one measured for the thoracic aorta (1.9). The present study demonstrates the utility of the DIC to determine the local strain fields and to analyze the tissue failure mechanisms. Different rupture patterns were observed.

Keywords Aorta, full strain field, structural characteristics, failure pattern, Digital Image Correlation.

I. INTRODUCTION

Traumatic rupture of the aorta (TRA) is a leading cause of death after vehicle crashes. Crash injury databases indicate that TRA accounts for about 20% of fatalities [1]. The overall survivability of such injury is less than 5% with a fatality rate of approximately 90% on the accident scene [2][3]. Although TRA is observed in different accident scenarios, the injury patterns are very similar among the victims. Currently, the most common site of TRA is located at the isthmus region [4]–[7]. While the exact injury mechanisms still remain unidentified, it is assumed that several mechanisms are involved in the failure of the aorta. Considering data from autopsy or surgery, the intima layer was identified as the first aorta's wall layer involved in the rupture. Moreover, the rupture is typically transverse to the longitudinal axis [8]–[10].

Several studies were conducted to validate specific hypotheses related to TRA. For instance, the effect of heart displacement was investigated by [5], and one of the conclusions was that anterior stretching of the thoracic aorta is one component of TRA injury mechanism. Various dynamic blunt loadings were performed on Post Mortem Human Subjects [11] to measure the motion and deformation of the aorta using a dynamic X-Ray device. These authors assumed that axial elongation (longitudinal stretch) of the aorta is an important cause for the generation of TRA. More specific studies focused on the mechanical properties of the arterial wall that are necessary for the understanding and modeling of TRA that occurs in car crashes.

In the literature, some works were dedicated to link the mechanical and structural properties of the aorta. Reference [12] tested up to failure different segments taken from thoracic and abdominal aortas and performed histological evaluation with quantification of morphometric parameters and composition of the entire vessel and its layers (media and adventitia). Regional differences in stiffness and failure parameters at physiological, low and high loading associated with significant differences and changes in the structure among the different layers and segments were reported. Other studies determined the mechanical properties along the aorta's length [13] and concluded that the higher stiffness and strength of the distal tissue are due to the different

S. Litlzer is PhD student in Biomechanics at University of Lyon, F-69622, Lyon, France; IFSTTAR, LBMC, UMR_T9406, F-69675, Bron; University Lyon 1, Villeurbanne. P. Vezin is senior researcher in Biomechanics at University of Lyon, F-69622, Lyon, France; IFSTTAR, LBMC, UMR_T9406, F-69675, Bron; University Lyon 1, Villeurbanne. (+33 472 142 379, +33 472 376 837, philippe.vezin@ifsttar.fr).

orientation of elastin along the aorta, i.e. a higher proportion of circumferentially-oriented fibres.

In addition to standard material characterization methods, non-contact optical methods were applied for evaluating the mechanical properties of soft tissues. Displacements can be measured by applying artificial markers to the tissue and monitoring their position during mechanical loading. Multiple-point regular grid on the surface of tissues was used to evaluate the mechanical properties of blood vessels [23][14]-[16]. The assumption in this approach is that the mechanical response is uniform and homogeneous between the markers. However, due to the complex structure of the arterial tissue composed of three layers of elastin and collagen, there is a high degree of non-linearity in response to large strain [17]. Local variation in the anisotropy and inhomogeneity of arterial tissues has not been fully examined in detail, partly due to the limitations of most experimental techniques that have been adopted for analysis.

In the present study, Digital Image Correlation (DIC) was adopted to determine the strain distribution in specimens of pig aorta subjected to uniaxial tension. DIC is a non-contact optical method that consists of following the random speckle pattern at the surface of the tested specimen, thanks to two digital cameras with incidence angles during deformation. DIC has been adopted to examine the deformation of structures [18][19] or the mechanical behavior of engineering materials [20][21]. More recently, this technique was used to determine the local strain field of soft tissue. It was used to evaluate the mechanical behavior of arterial tissue on bovine aorta [22] and to characterize the failure in aneurismal human aortic tissue [23]. A complete description of the DIC technique can be found in [24].

This study is part of a research project to develop a biofidelic numerical model able to reproduce the rupture of the aorta under car crash loading conditions. The study attempts to obtain experimentally the full strain field up to failure of the inner layer of the aorta under dynamic loading and visualize the evolution of the rupture to the other layers. The influence of the location along the aorta was assessed in terms of maximum load, strain and stress. The characteristics, initiation and propagation of the rupture are discussed.

II. METHODS

Specimen preparation

Seven healthy aortas were removed from 6 month old pigs just after euthanasia. The pigs come from a local abattoir and are standard pigs for consummation. The whole aortas were wrap in moist paper and immediately stored in the freezer (-18°C) until their use. Frozen aortas were thawed at room temperature (19°C) three hours before their preparation. Connective and adipose tissue were gently removed from the surface of the adventitia by blunt dissection with surgical scissors. Aortas were opened along the longitudinal direction using surgical scissors. About ten (depending on size and condition of the aortas) specimens were cut into a dog bone shape using a punch and a manual press along their longitudinal orientation. All sampling procedures were carried out in accordance with the guidelines of the IFSTTAR-LBMC laboratory for biological material handling. The specimens were taken at four different locations along the aorta from the aortic arch (location 1) to the abdominal aorta (location 4). The typical dimensions of samples, the location and the denomination of each sample in accordance with their location are presented in Fig. 1.

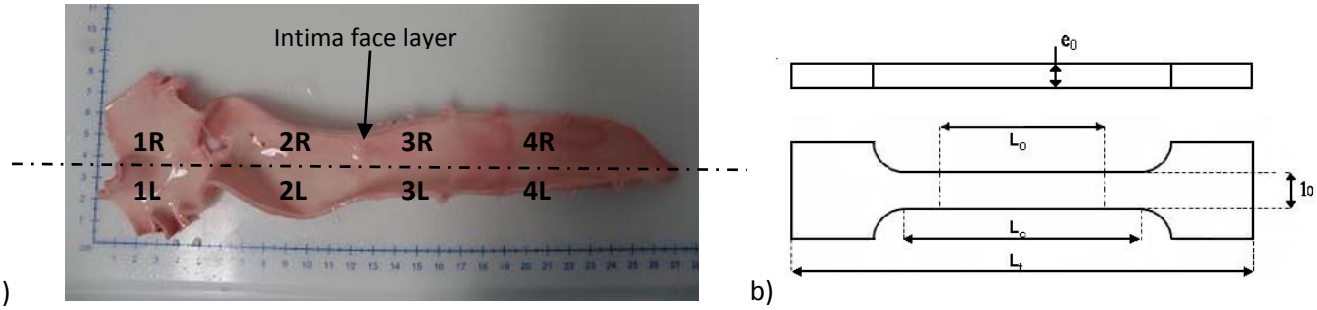

a) b)

Fig. 1. a) Longitudinal cutting of pig aorta and location of specimens. b) Dimensions of specimen: useful width (l_0=6mm), useful length (L_0=13 mm), calibrated length (L_c=15 mm) and total length (L_t=45 mm). Location 1 is at the aortic arch, location 4 at the abdominal aorta, L and R correspond to left and right respectively.

The thickness (e_0) of the useful length for each sample was measured just after cutting by a calliper with an accuracy of ± 0.01 mm and is given in Table I according to the location of each sample. Before and during the testing phase, all samples were kept under moist paper with physiological saline solution to ensure their hydration at room temperature.

TABLE I THICKNESS OF EACH SAMPLE

AORTA N°	THICKNESS (MM)							
	1L	*1R*	*2L*	*2R*	*3L*	*3R*	*4L*	*4R*
5	2.33	2.46	2.13	2.08	1.78	1.68	1.55	1.43
6	2.03	1.95	1.98	2.05	1.68	1.63	1.20	1.30
7	2.00	2.10	2.00	1.95	1.45	1.48	--	--
8	2.05	-	2.20	2.18	1.75	1.90	1.53	1.50
9	2.25	2.13	2.10	1.95	1.73	2.23	1.48	1.38
10	2.28	2.65	2.25	2.23	1.53	1.58	1.43	1.63
11	2.33	2.35	2.05	1.93	1.53	1.65	1.50	1.45
Mean	2.18	2.27	2.10	2.20	2.05	1.63	1.91	1.73
S.D.*	±0.15	±0.26	±0.10	±0.11	±0.12	±0.13	±0.19	±0.25

**S.D.: Standard Deviation*

Tensile tests

Tensile tests were performed using a universal tensile test machine (Instron® 8802). Samples were fixed using specially designed clamps. Sandpaper was glued on the clamp to prevent the slipping of a sample that can occur in ordinary grips. Prior to the test, a rod was fixed to inferior and superior clamps to ensure no pre-stretching of samples. This rod was removed just before preconditioning (Fig. 2.).

Each specimen was preconditioned first by applying a load of 0.5 N and then 5 cycles of small amplitude (0.5mm) at 1 Hz. Then the aortic specimen was subjected to dynamic loading up to failure at a constant strain rate of about 68 s^{-1} (velocity of the cross-head of the tensile machine was 1 $m.s^{-1}$). The tensile load was measured with a 1 KN piezoelectric load cell. The accuracy of the load cell was 0.5% of the measured values (channel class 0.5). The elongation l was calculated via the displacement cell attached to the cross-head. The data were continuously recorded at a frequency of 5,000 Hz with the Instron® on-board software.

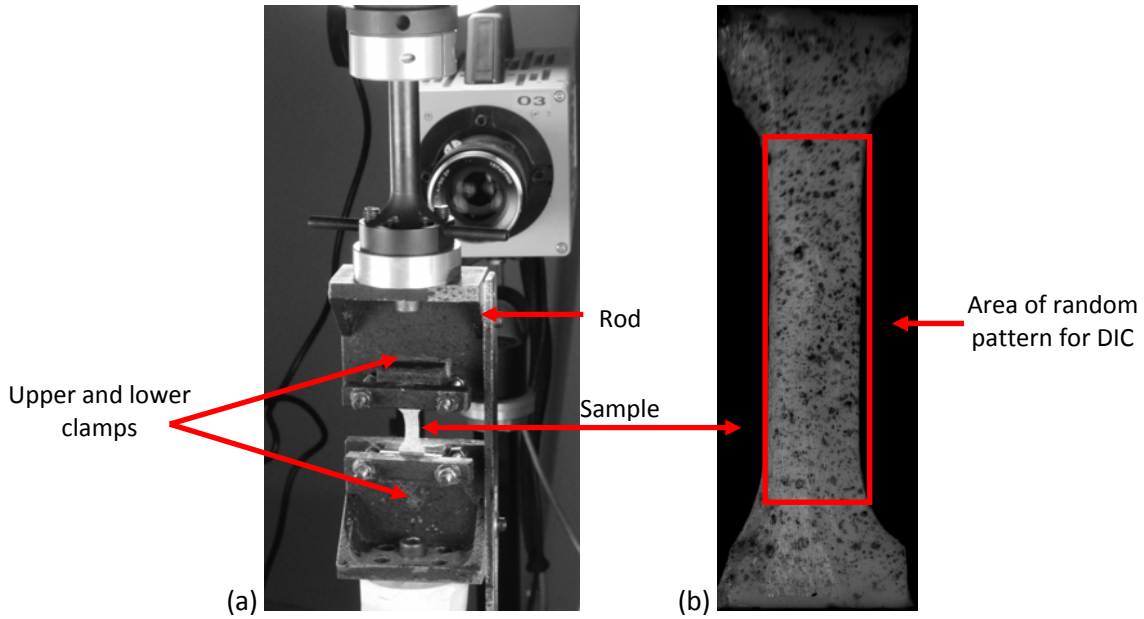

Fig. 2. Aortic specimen fixed on the clamps mounted on universal test machine (a). Example of a random pattern on the intima layer for Digital Image Correlation (b).

Digital Image Correlation

Digital Image Correlation (DIC) technique was used to obtain the strain full-field on the surface of the intima layer. DIC [24] consists of following the random speckle pattern at the surface of the tested specimen, thanks to two digital cameras with incidence angles during deformation. Two high speed Photron Fastcam SA3® digital video cameras with an image size of 1024x1024 pixels² were used to record the sample evolution during the test. Two 105 mm macro lenses were used to have appropriate size and depth of field in accordance with small samples tested. The cameras' speed acquisition was 4,000 f.s^{-1}.

The random speckle pattern was applied on the intima layer with a black paint which was sprayed horizontally, leaving fine particles to fall vertically on the sample lying on a horizontal plane. A black pattern was chosen due to the white colour of the aorta. The stereo-correlations were based on the pair of images and processed using VIC3D® software (Version 2009—Correlated Solution, Inc.) to obtain the displacement field at every node of a 7 px (0.27 mm) grid using 21 × 21 px2 (0.81 × 0.81 mm²) patterns that covered successively the whole 6×13 mm² patterns that covered the tissues. Then the software computed the Green-Lagrange strain field (accuracy around 0.01 – 0.02%). Prior to the test, the VIC3D® software was calibrated with the record of the pictures of a calibration object (grid of 9x9 markers, with 2 mm spacing) that covered the area of sample deformation.

Data analysis

The load-stretch curve was derived to obtain the true stress-true strain relationship. This method takes into account the large deformation of the specimen and subsequently the actual change of its dimension during testing. The aortic wall was assumed to be an incompressible material [25]. True strain and stress (i.e. Cauchy stress) were obtained from engineering strain and stress respectively. The engineering strain and stress are:

$$\sigma_E = \frac{F}{S_0}, \text{ and } \quad \varepsilon_E = \lambda - 1 \text{ with } \quad \lambda = \frac{l}{L_0} \tag{1}$$

where F is the load applied, $S_0 = l_0 \times e_0$ is the initial cross-sectional area, λ is the stretch ratio and L_0 the initial length. True strain and stress are computed as follows:

$$\sigma = \sigma_E(1+\varepsilon_E), \text{ and } \varepsilon = \ln(1+\varepsilon_E) \tag{2}$$

The maximum load and true stress were determined and compared between the specimens.

In addition to this classic strain-stress analysis, the full strain field obtained from the DIC analysis is used to determine the maximum Green-Lagrange (GL) strain value just before the initiation of the first rupture. The longitudinal strain E_{zz} obtained by this method is also compared with the value derived from the stretch ratio or engineering strain using the relationship:

$$E_{zz} = \frac{1}{2}(\lambda^2 - 1) = \varepsilon_E(1 + \frac{\varepsilon_E}{2}) \tag{3}$$

Statistical analysis

A statistical study was completed to determine the effect of location on the tissue strain and stress. Data from the aortas were grouped by location and the differences between the four groups were assessed with Student *t*-test. Significance was assumed at a *p* value <0.05. In some cases, a non-parametric Wilcoxon matched-pairs signed-ranks test (2-tailed at a significance level of p = 0.05) was used to increase the sensitivity of the analysis by exploiting the fact that the results could be paired.

III. RESULTS

Fifty three specimens were obtained from seven pigs. Eight to ten different locations along the aorta were tested for each pig in the longitudinal direction (Table I). The possible slippage was checked visually on the video and by comparison of the stretch ratio determined from the cross-head displacement and those measured by DIC. No significant slippage was observed and all the specimens were tested. For each tensile test performed a force-displacement curve was obtained. The true stress and the true strain were then calculated using equation (2) and strain-stress relations were plotted for each specimen. Two examples from two different locations and pigs are shown in Fig. 3 to illustrate the variability between pigs and location. Fig. 3.a represents typical true stress vs. true strain curves and Fig. 3.b shows typical engineering stress vs. engineering strain curves. Moreover, the stress-strain curves show the non-linearity of the mechanical response to loading as well as the onset of the failure.

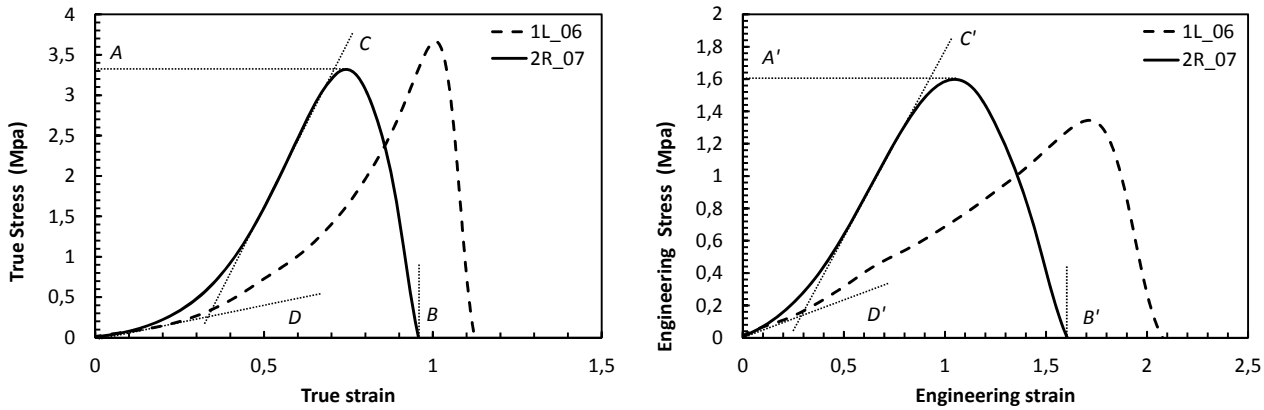

Fig. 3. Typical stress-strain graph from the experiments:
a) True stress-true strain curves, b) Engineering stress-engineering strain curves.
The ultimate true and engineering stress are the maximum stress until failure of the specimen and are indicated by A and A' respectively. The global failure true strain and engineering strain are the maximum strain obtained before failure and are shown by B and B' respectively. The slope of the curve at large strain and the initial slope at small strain are shown by C (C') and D (D') respectively.

Paired comparisons were performed to assess the thickness variation along the aorta. The results showed that there were no significant thickness differences between left and right sides of the specimens for the same location (p>0.05 for all comparisons). The average thickness decreased from the aortic arch to the bottom of the aorta. The thickness at location 4 was found significantly lower (p<0.0001) than the three other locations. Thickness at location 3 was also found significantly lower than locations 1 and 2 (p<0.01, except for 3R-2L comparison where p<0.042). However, there was no significant difference between locations 2 and 1 (aortic arch).

Maximum load and stress

The maximum force $F_{\max}$ and ultimate true stress (UTS) value at the failure of the specimens were defined from the force-stretch curves and true stress- true strain curves respectively. The ultimate engineering stress (UES) was computed from the maximum load using equation (1). $F_{\max}$, UTS and UES were compared with respect to their location on the aorta. For that purpose, right, *iR*, and left, *iL* (see Fig.1.a) specimens were grouped for the same longitudinal location (*Gi*=*iR*+*iL* samples, with *i*=1,4). Fig. 4 and Fig. 5 summarize the average values for the four different locations.

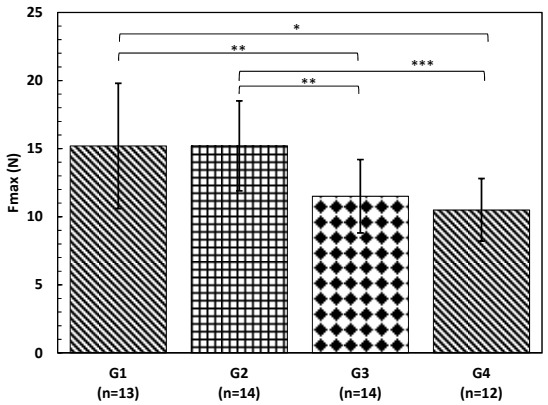

Fig. 4. Mean and standard deviation of maximum load for the four locations
(G1, G2, G3 and G4 correspond to the four groups of data for the four locations).
Asterisks represent significant differences (*: p<0.05, ** p<0.005, ***p<0.001)

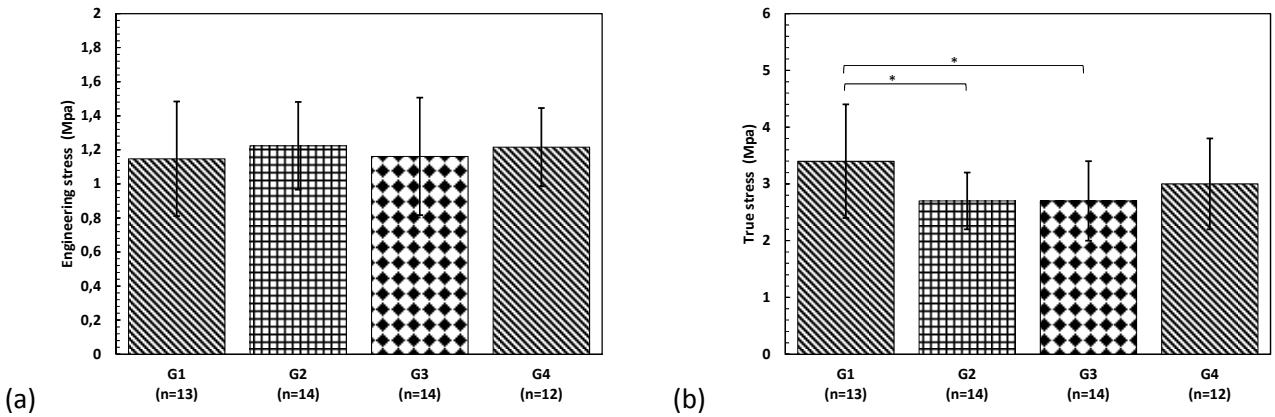

Fig. 5. Mean and standard deviation of ultimate engineering stress (a), ultimate true stress (b), for the four locations. Asterisks represent significant differences (*: p<0.05)

The effect of the location on the maximum load was found significant for the comparison between *G1* and *G3* (p=0.016) and for *G1 vs*. *G4* (p=0.004) as well as for *G2 vs*. *G3* (p=0.003) and *G4* (p<0.001). This effect was not observed for the comparison between two adjacent locations: *G1 vs*. *G2* and *G3 vs*. *G4*. These results show a decrease of the maximum load from the aortic arch to the abdominal part of the aorta.

There was no significant influence of the location on the UES values. On the other hand, an influence of the location on the UTS values was found significant for *G1* compared to *G2* and *G3* with a p value of 0.041 and 0.033 respectively. However, the comparison of the UTS values at the *G4* location with the three other locations did not show significant effect of the location (p>0.25). A similar trend was observed for *G2 vs. G3.*

Strain data from Digital Image Correlation

An interesting feature of DIC is its ability to calculate local strain compared to the global strain obtained from the displacement sensor. Fig. 6 shows an example of DIC analysis. From the DIC analysis it was found that a local amplification of the local GL strain occurred just before the failure of the aortic tissue close to the rupture site on the intima. The rupture of the intima was detected on the video sequence (4 frames on the right side of Fig. 6.). Then, the local maximum GL strain (LMS) was extracted from the frame just before the initiation of the rupture of the intima (left frame on Fig. 6.). These values of the LMS just before rupture are given in Table II.

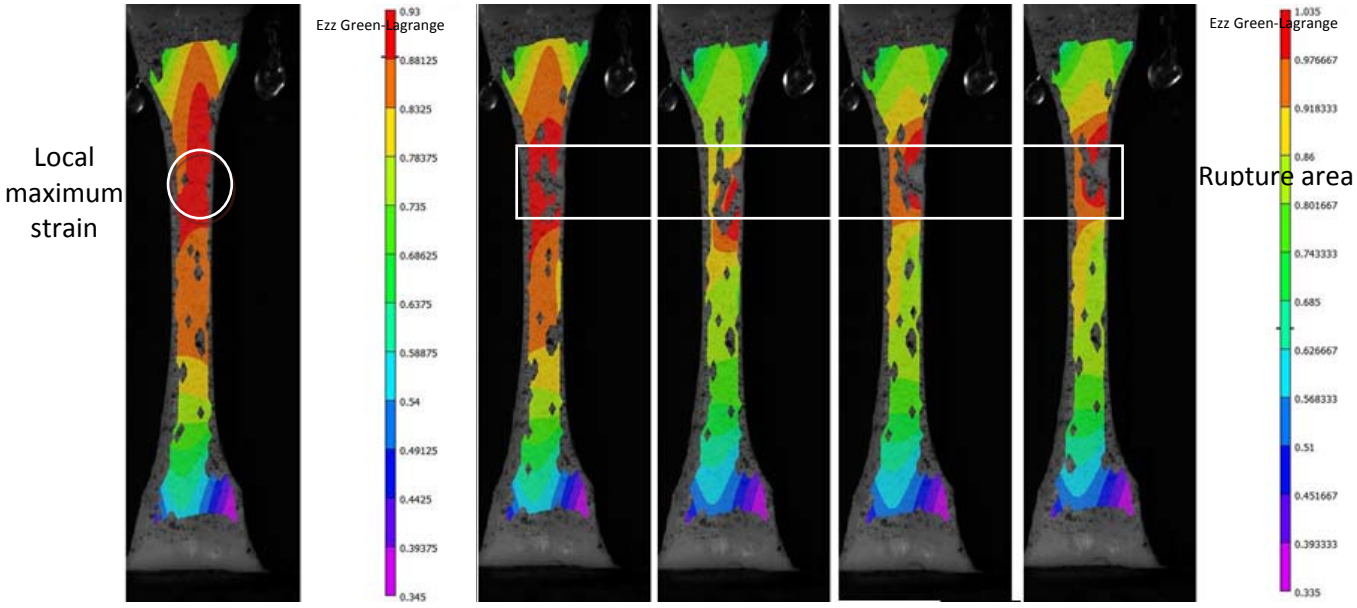

Fig. 6. Example of Green-Lagrange strain field at rupture from Digital Image Correlation analysis.

TABLE II LOCAL MAXIMUM VALUES OF THE GREEN-LAGRANGE STRAIN AT BEGINNING OF THE FAILURE

AORTA N°	*1L*	*1R*	*2L*	*2R*	*3L*	*3R*	*4L*	*4R*
5	1.83	2.15	1.36	0.94	1.02	2.06	1.98	2.2
6	1.6	1.11	0.82	1.22	1.58	1.42	1.54	1.6
7	2.55	3.42	1.11	1.07	1.64	2	--	--
8	1.68	--	1.04	1.33	0.74	0.86	1.87	1.56
9	2.2	2.45	1.40	1.18	0.88	0.86	1.8	1.73
10	1.68	2.43	1.25	1.39	1.34	1.25	1.69	1.43
11	1.32	1.74	0.71	0.72	1.28	1.16	1.57	1.88

The MLS values were also grouped by location and the influence of the position along the aorta was statistically assessed. Differences were found significant for the comparisons *G1 vs. G2* (p<0.0002) and *G3* (p=0.0014), as well as for *G4 vs. G2* (p<0.0001) and *G3* (p=0.002). On the contrary the influence of the location was not found significant for the comparison of *G2* with *G3* (p=0.181) and *G1* with *G4* (p=0.148).

By comparison, the values of the global GL strain obtained with equation (3) were found to be higher (almost twice) than the values computed from the DIC (Table III). Moreover, the influence of the location on the global strain value was not found to be significant for all the comparisons between *G2*, *G3* and *G4*. The comparison of *G1* with the three others shows significant differences (p<0.0002).

TABLE III COMPARISON OF THE AVERAGE AND STANDARD DEVIATION VALUES OF THE GLOBAL AND LOCAL MAXIMUM GREEN-LAGRANGE STRAIN AT FAILURE

°	*1L*	*1R*	*2L*	*2R*	*3L*	*3R*	*4L*	*4R*
LOCAL	1.84	2.22	1.09	1.12	1.21	1.37	1.74	1.73
	±0.41	±0.77	±0.26	±0.23	±0.34	±0.49	±0.17	±0.27
GLOBAL	3.79	4.23	2.04	1.89	2.17	2.37	2.60	2.53
	±0.66	±1.02	±0.90	±0.62	±1.08	±0.91	±1.06	±0.61

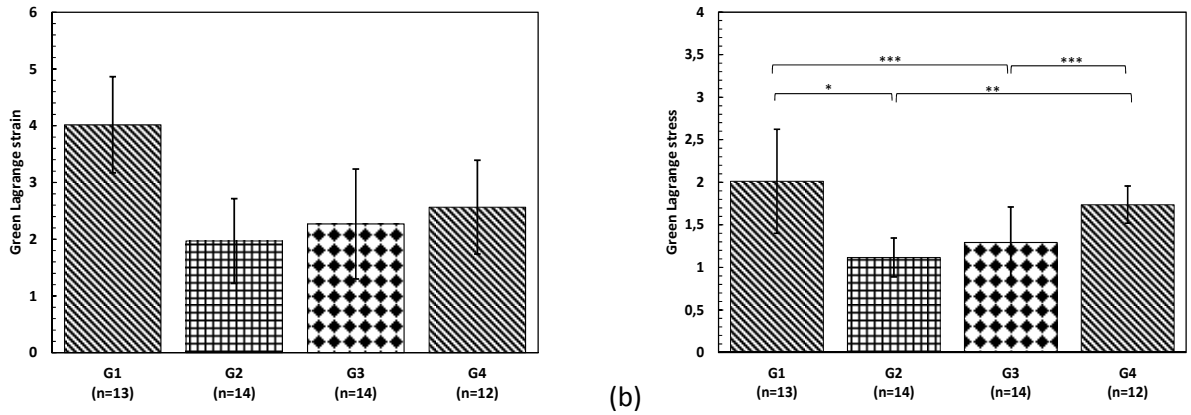

(a) (b)

Fig. 7. Mean and standard deviation of Green-Lagrange strain for the four locations: (a) Global strain computed from stretch ratio (b), local strain from Digital Image Correlation.
Asterisks represent significant differences (*: p<0.0002, ** p<0,0001, *** p<0,002)

IV. DISCUSSION

Effect of the location on the ultimate stress

Rupture of the aorta is a leading cause of death after vehicle crashes, but the exact injury mechanisms remain still unidentified. Computational assessment of traumatic rupture of the aorta is one of the main challenges to improve the assessment of vehicle safety. Knowledge of aortic wall behavior is critical in improving the biofidelity of computational analysis and a correct description of the mechanical properties up to failure is needed. The mechanical parameters of the aortic wall have been intensively studied in the past using uniaxial or biaxial tensile testing ([10][12][26]-[28]).

True stress-engineering strain and engineering stress-engineering strain relationships have been published. However, these traditional approaches do not give a true indication of the deformation characteristics of the soft tissue since they are based on the original dimensions of the specimen and not on the actual dimensions during the test. This is particularly critical for the aortic tissue under uniaxial loading that undergo large stretch due to their hyper-elastic behavior. The actual variation of the current cross-sectional area of the tissue must be taken into account and hence, under the assumption of the incompressibility of the tissue, the true stress-true strain relationship was used in the present study.

Our results show the regional change of the aortic wall thickness that gradually decreased from the aortic arch to the abdominal aorta. This is in good agreement with aortic morphometric studies [12]. These authors report that wall thickness decreases down the thoracic part of the aorta and remains constant in the abdominal one. This decrease in the overall thickness is due to the decrease of the media thickness whereas the adventitia thickness remains constant. In the abdominal aorta, the media thickness decreases more slowly and is compensated by an increase of the adventitia thickness by about the same amount.

The comparison between the different locations along the aorta showed significant difference for the ultimate load ($F_{\max}$). The ultimate force decreases from the aortic arch to the abdominal aorta. This should be put together with the decrease of the thickness of the aorta wall in the same direction. When comparing the ultimate engineering stress that takes into account the thickness of the arterial wall, the influence of the location was not found significant. All the specimens whatever their position along the descending aorta have the same ultimate engineering stress. However, when the same analysis was performed on the true stress that not only takes into account the initial-cross section but also its variation during the loading, an influence of the spatial location was observed. This comparison between engineering and true stresses suggests that the regional thickness variation is not the cause of the decrease of the ultimate stress.

Structural parameters such as orientation and number of elastin and collagen fibres are probably factors of influence. The true stress takes into account the modification of the structure of the arterial wall due to the successive recruitment of the collagen fibres during the loading. The distribution and orientation of these fibres were found to vary along the aorta [12]. This author explained that the wall of the aortic arch had the highest elastin area density whereas the abdominal aorta had the lowest. The relative area of density of collagen was almost constant in the thoracic part of the aorta and steadily increased down the abdominal aorta.

In addition to these differences in the density of components, there is also a difference in the material properties. The collagen's Young's modulus is greater than the elastin one [29]. Consequently, the stretch and then the ultimate stress of the arterial tissue are affected by the ratio elastin/collagen. The orientation of the fibres is also an important parameter that can explain the differences between the locations along the aorta. A structural model was proposed by [30] who measured the orientation of the collagen fibers in the three layers of the arterial wall. This author found that these fibres are oriented with respect to the transverse direction by an angle of 18.8° (intima), 37.8° (media) and 58.9° (adventitia) respectively. In our study, the ultimate tensile stress in the longitudinal at the aortic arch was found to be slightly greater than for the different locations along the descending aorta. Reference [29] reports an opposite trend for the circumferential ultimate tensile stress. This difference between longitudinal and circumferential material properties behavior is due to the non-isotropic properties of the aortic wall and to the orientation of the collagen fibres.

Failure pattern of the aortic wall to uniaxial loading

The digital image correlation methodology used in the present work allows us to determine the full-field strain at the intima surface of the aorta. This approach compared to the traditional one permits access to the local values of the strain. Thanks to the DIC, the different steps of the failure of the intima layer were observed qualitatively on the digital image and the local magnification of the strain close to the starting point of the rupture was quantified.

The Green-Lagrange ultimate strain values obtained from the DIC were found lower than the global values computed from the displacement sensor mounted on the tensile machine. The DIC analysis provides the strain at the surface of the intima layer while the global values are a measure of the whole arterial wall elongation. The intima layer is known to be more fragile than the media and the adventitia. A similar study with speckle pattern of the adventitia side of the aorta needs to be performed. An attempt was made to apply DIC on both sides of the specimen. This was not successful due to the difficulty to apply a random speckle pattern on both sides without creating artifacts (pattern on one side are visible on the other side by transparency).

The local maximum longitudinal strain was found significantly different and higher at the aortic arch compared to the descending aorta (Wilcoxon matched-pairs signed-ranks test). This result implies that the

aortic wall is less extensible from the aortic arch to the abdominal one. This is consistent with previous observational reports in the literature [12]. The same research group suggested that at high stresses the mechanism of the elongation of the tissue is controlled by the straightening of the collagen fibres [31].

In the majority of the cases, the failure of the tissue starts close to the point of the maximum Green-Lagrange strain. The intima is torn locally and the failure propagates transversely horizontally or with an angle along the width of the specimen (Fig. 8). The aortic tissue continues to be stretched and then the whole arterial wall suddenly breaks. Depending on the specimens, the total rupture happens either rapidly after the tear of the intima or later with a substantial elongation of the specimen. Due to the absence of the speckle pattern once the intima is broken, the strain just before the total rupture cannot be determined. Multiple tears of the intima are sometimes observed on the specimen but almost with the same pattern with finally a rupture of the specimen at the maximum strain location.

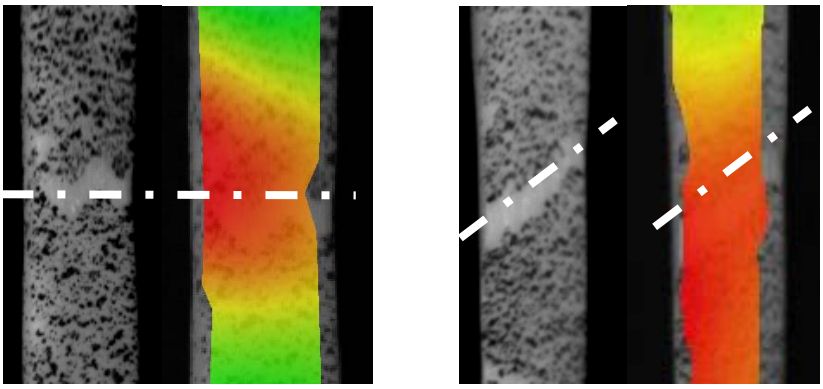

a) Horizontal propagation b) inclined propagation

Fig. 8. Examples of different types of aortic wall failure.
The red color corresponds to the maximum of Green-Lagrange longitudinal strain.

The inclined propagation of the rupture was already observed for other soft fibrous tissues such as the skin or the liver capsule [32][33]. These authors explained that the failure pattern is linked with the micro structure of the tissues and more specifically with the orientation, recruitment and rearrangement during the loading of the collagen fibres. To support their assumption they performed histological analysis that was not possible on our aortic samples.

Limitation of the study

As with many other soft tissues, the arterial wall mechanical properties are strain rate dependent. The present study was performed at a constant strain rate of 68 s^{-1} (constant loading speed of 1m.s^{-1}). For better assessment of the mechanical properties and failure mechanism, additional data need to be acquired at different strain rate. Moreover, this study focused only on uniaxial loading. A biaxial tensing test could be more appropriate to take into account the radial deformation of the aortic wall due to internal pressure or arterial dilation. The assumption of quasi-incompressibility of the arterial wall to compute the stress and the strain from the measured stretch is questionable. The incompressibility was demonstrated in the past under loading in the range of the physiological conditions [25][34][35], but the applicability of this assumption at higher magnitudes of stress or strain is not yet demonstrated and could depend on the loading and deformation applied to the tissues [36]. Another problem with *in vitro* tissue testing compared to real loading in the human body is the absence of the pressure of the surrounding organs. The applied loading in our research is a simplification of the forces actually being applied to the aorta. A study on the rat carotid artery demonstrated that the mechanical properties of the rat carotid artery substantially differ *in vivo*, *in situ* and *in vitro* [37].

The present study was performed on a relatively small sample size (n<15). In order to achieve statistical power, the left and right specimens at the same location from each aorta were regrouped. Consequently, we assumed that there were no effects of the laterality. Only a few tests (4) were rejected due to tissue slippage. Additional tests need to be performed to increase the statistical power and to assess the effect of the laterality.

Concerning the DIC analysis, the main difficulty comes from the achievement of the speckle pattern on soft tissue. This is particularly difficult on small aortic specimens. In some cases, the random speckle pattern was not good enough in terms of contrast, isotropy and non-periodicity to obtain a good correlation. Nevertheless, the DIC method is a very accurate method and was used in the last decades by several research teams to obtain

experimentally a mapping of the strain on biological soft tissues, see for instance [22][23][32][33][38]. With such information, we can then compute the full field stress and determine a reliable model of the arterial wall up to failure. Such a model taking into account the anisotropy, heterogeneity and structural parameter of the aorta can be implemented in the FE model.

V. CONCLUSIONS

In order to study the mechanisms of traumatic rupture of the aorta, we performed an experimental study to determine the stress-strain relationships up to failure along the descending thoracic aorta. Fifty-three pig aorta specimens were submitted to longitudinal loading at a constant strain rate of 68 s^{-1}. Cauchy stress-true strain curves were derived from the force-displacement measurements and Digital Image Correlation method was applied to determine the full-field strain at the surface of the intima.

We analyzed the effect of the location along the descending aorta. Our results show that the maximum load at failure decreased from 15.2N to 10.5N with the location, i.e. from the aortic arch to the abdominal aorta. On the other hand, the engineering stress at rupture was found to be similar whatever the location (about 1.2±0.3 MPa). But significant influences of the location were found for the Cauchy stress (3.4MPa at the aortic arch, 2.7MPa for the thoracic aorta and about 3.0MPa for the abdominal aorta). This result can be explained by the differences in the micro structure such as orientation and number of collagen fibers that are described in the literature.

The analysis of the strain field by DIC shows that the aortic arch encountered large Green-Lagrange strain (4.0) compared to the descending aorta where influence of location has been observed (Green-Lagrange strain at failure increases from 1.9 (thoracic aorta) to 2.6 (abdominal aorta).

Finally, two common types of failure pattern were identified: a typical inclined failure pattern that propagates continuously up to the final failure of the tissue and a horizontal and sudden rupture of the arterial wall.

VI. REFERENCES

[1] Richens D, Kotidis K, Neale M, Oakley C, Fails A, Rupture of the aorta following road traffic accidents in the United Kingdom 1992—1999. The results of the co-operative crash injury study, *European Journal of Cardiothoracic Surgery*, 23, 2, 143-148, 2003.

[2] Richens D, Field M, Neale M, Oakley C, The mechanism of injury in blunt traumatic rupture of the aorta, *European Journal of Cardiothoracic Surgery*, 21, 2, 288-293, 2002.

[3] Jamieson WRE, Janusz MT, Gudas VM, Burr LH, Fradet GJ, Henderson C, Traumatic rupture of the thoracic aorta: Third decade of experience, *American Journal of Surgery*, 183, 5, 571-575, 2002.

[4] Greendyke RM, Traumatic rupture of the aorta; special reference to automobile accidents, *The Journal of the American Medical Association*, 195, 527-530, 1966.

[5] Bertrand S, Cuny S, Petit P, Troseille X, Page Y, Guillemot H, Drazetic P, Traumatic rupture of thoracic aorta in real-world motor vehicle crashes, *Traffic injury prevention*, 9, 153-161, 2008.

[6] Siegel JH, Smith JA, Siddiqi SQ, Change in velocity and energy dissipation on Impact in motor vehicle crashes as a function of the direction of crash: Key factors in the production of thoracic aortic injuries, their pattern of associated injuries and patient survival. A crash injury research engineering network (CIREN) Study, *The Journal of Trauma Injury Infection and Critical Care*, 57, 4, 760-778, 2004.

[7] Katyal D, McLellan BA, Brenneman FD, Boulanger BR, Sharkey PW, Waddell JP, Lateral impact motor vehicle collisions: significant cause of blunt traumatic rupture of the thoracic aorta, *The Journal of Trauma Injury Infection and Critical Care*, 42, 5, 769-772, 1997.

[8] Sevitt S, The mechanisms of traumatic rupture of the thoracic aorta, *British Journal of Surgery*, 64, 3, 166-173, 1977.

[9] Viano DC, Biomechanics of non-penetrating aortic trauma: a review, *Proceeding of the 27th Stapp Car Crash Conference,* San Diego CA USA, 109-114, 1983.

[10] Shah CS, Hardy WN, Mason MJ, Yang KH, Dynamic biaxial tissue properties of the human cadaver aorta, *Stapp Car Crash Journal*, 50, 217-246, 2006.

[11] Hardy NH, Shah CS, Mason MJ, Kopacz JM, Yang KH, King AI, Van Ee A, Mechanisms of traumatic rupture of the aorta and associated peri-isthmic motion and deformation, *Stapp Car Crash Journal*, 52, 233-265, 2008.

[12]Sokolis DP, Passive mechanical properties and structure of the aorta: segmental analysis, *Acta Physiologica*, 190, 4, 277-289, 2007.
[13]Lillie MA, Gosline JM, Mechanical properties of elastin along the thoracic aorta of pig. *Journal of Biomechanics*, 40, 2214-2221, 2007.
[14]Zhou J, Fung YC, The degree of nonlinearity and anisotropy of blood vessel elasticity. *Proceeding of the National Academy of Sciences of the United States of America,* 94, 26, 14255-14260, 1987.
[15]Humphrey JD, Vawter DL, Vito RP, Quantification of strains in biaxially tested soft tissues, *Journal of Biomechanics*, 20, 1, 59-65, 1987.
[16]Stemper BD, Yoganandan N, Pintar FA, Methodology to study intimal failure mechanics in human internal carotid arteries, *Journal of Biomechanics*, 38, 12, 2491-2496, 2005
[17]Silver FH, Christiansen DL, Buntin CM, Mechanical properties of the aorta: A review, *Critical Reviews in Biomedical Engineering*, 17, 4, 323-358, 1989.
[18]Chu TC, Ranson WF, Sutton MA, Peters WH, Application of Digital-Image-Correlation technique to experimental mechanics, *Experimental Mechanics*, 25, 3, 232-24, 1985.
[19]Sutton MA, Chao YJ, Lyons JS, Computer vision methods for surface deformation measurements in fracture mechanics, Novel experimental techniques in fracture mechanics, *Proceeding of the ASME Winter Annual Meeting AMD*, New Orleans LA USA, 176, 203-2017, 1993.
[20]Zhao W, Jin G, An experimental study of measurement of Poisson's ration with digital correlation method, *Journal of Applied Polymer Science*, 60, 8, 1083-1088, 1996
[21]Zhang D, Zhang X, Cheng G, Compression strain measurement by digital speckle correlation, *Experimental Mechanics*, 39, 1, 62-65, 1999.
[22]Zhang D, Eggleton CD, Arola DD, Evaluating the mechanical behavior of arterial tissue using Digital Image Correlation. *Experimental Mechanics*, 42, 4, 409-416, 2002.
[23]Kim JH, Badel P, Duprey A, Favre JP, Avril S, (2011) Characterization of failure in human aortic tissue using digital image correlation. *Computer methods in Biomechanics and Biomedical Engineering*, 14, S1, 73-74, 2011.
[24]Sutton M, Orteu J, Schreier H, Image correlation for shape, motion and deformation measurements: Basic concepts, theory and applications. 364 p., *Springer*, New York, 2009.
[25]Carew TE, Vaishnav RN, Patel DJ, Compressibility of the arterial wall. *Circulatory Research*, Volume 23, Issue 4, pp. 61-8, 1968.
[26]Mohan D, Melvin JW, Failure Properties of Passive Human Aortic Tissue, II-Uniaxial Tension Tests, *Journal of Biomechanics*, 15, 11, 887-902, 1982.
[27]Mohan D, Melvin JW, Failure Properties of Passive Human Aortic Tissue, II-Biaxial Tension Tests, *Journal of Biomechanics*, 16, 1, 31-44, 1983.
[28]Bass CR, Darvish K, Bush B, Crandall JR, Srinivasan S, Tribble C, Fiser S, Tourret L, Evans JC, Patrie J, Wang C, Material properties for modeling traumatic aortic rupture, *Stapp Car Crash Journal*, 45, 143-160, 2001.
[29]Pearson R, Philips N, Hancock R, Hashim S, Field M, Richens D, McNally D, Regional wall mechanics and blunt traumatic aortic rupture at the isthmus, *European Journal of Cardiothoracic Surgery,* 34, 616-622, 2008.
[30]Holzapfel G, Determination of material models for arterial walls from uniaxial extension tests and histological structure, *Journal of Theoretical Biology,* 238, 290–302, 2006.
[31]Sokolis DP, Kefaloyannis EM, Kouloukoussa M, Marinos E, Boudoulas H, Karayannacos PE, A structural basis for the aortic stress–strain relation in uniaxial tension, *Journal of Biomechanics,* 39, 9, 1651–1662, 2006.
[32]Brunon A, Bruyère-Garnier K, Coret M, Mechanical characterization of liver capsule through uniaxial quasi-static tensile tests until failure. Journal of Biomechanics 43, 11, 2221-2227, 2010.
[33]Ní Annaidh A, Bruyère K, Destrade M, Gilchrist MD, Otténio M, Characterising the anisotropic mechanical properties of excised human skin. *Journal of the Mechanical Behavior of Biomedical* Materials 5, 1, 139-148, 2012.
[34]Chuong CJ, Fung YC, Compressibility and constitutive equation of arterial wall in radial compression experiments, *Journal of Biomechanics*, 17, 1, 35–40, 1984.
[35]Girerd XJ, Acar C, Mourad JJ, Boutouyrie P, Safar ME, Laurent S, Incompressibility of the human arterial wall: an in vitro ultrasound study, *Journal of Hypertension*, 10, 6, 111-114, 1992.
[36]Volokh KY, Compressibility of arterial wall in ring-cutting experiments, *Molecular and Cellular Biomechanics*, 3, 1, 35-42, 2006.

[37]Zanchi A, Stergiopulos N, Brunner HR, Hayoz D, Differences in the mechanical properties of the rat carotid artery in vivo, in situ, and in vitro, *Hypertension*, 32, 1, 180-185, 1998.

[38]Brunon A, Bruyere-Garnier K, Coret M, Characterization of the nonlinear behaviour and the failure of human liver capsule through inflation tests, *Journal of the Mechanical Behavior of Biomedical Materials*, 4, 8, 1572-1581, 2011.